

## Pinpointing the macroscopic signatures of attosecond transient absorption in helium: Reshaped spectral splitting and persistent quantum beating

Jiajia Liu,<sup>1</sup> Wei Cao,<sup>1,\*</sup> Qingbin Zhang,<sup>1</sup> and Peixiang Lu<sup>1,2</sup>

<sup>1</sup>*School of Physics and Wuhan National Laboratory for Optoelectronics, Huazhong University of Science and Technology, Wuhan 430074, China*

<sup>2</sup>*Optics Valley Laboratory, Wuhan 430074, China*



(Received 30 January 2022; accepted 7 June 2022; published 21 June 2022)

Although attosecond transient absorption spectroscopy (ATAS) has been widely used in the study of ultrafast dynamics of atoms, molecules, and solids, there is a need for further theoretical exploration of macroscopic effects beyond the response of single atoms. Here, the extreme ultraviolet (XUV) absorbance of He atoms in the presence of a delayed near-infrared (NIR) pulse is studied theoretically, from the limit of dilute-gas medium to high densities. By numerically solving the time-dependent Schrödinger equation coupled with Maxwell's equations, we elucidate the macroscopic signatures in the absorption spectrum of an optically dense medium, including previously recognized XUV spectral pulse shaping, a complex spectral splitting, and a persistent quantum beating, based on the energies of the states involved. An analytical expression for optical density is deduced directly to pinpoint the physical origins of the various absorption features in a quantitative way, which helps one grasp the intuitive picture of the macroscopic absorption spectrum and provides guidance to explore applications such as optical pulse shaping and XUV molecular quantum beat spectroscopy.

DOI: [10.1103/PhysRevA.105.063515](https://doi.org/10.1103/PhysRevA.105.063515)

### I. INTRODUCTION

Attosecond transient absorption spectroscopy (ATAS) has been demonstrated to be capable of observing and manipulating ultrafast processes in atoms [1–3], molecules [4–8], and solids [9–12]. The advancements of this technique have led to a better understanding of many fundamental physical phenomena, including valence electron motion [13], autoionization dynamics, electromagnetically induced transparency (EIT) [14], formation of light-induced states [3,15,16], and line-shape modification [17,18].

However, in most of the studies of attosecond transient absorption measurements involving gas samples, the researchers treat the target gas as a thin medium even though many of these measurements were performed at relatively large optical densities. In fact, when the extreme ultraviolet (XUV) pulse propagates in a dense medium, the polarization created by the incident XUV is so strong that it can reradiate XUV light, and this newly generated light field can further excite secondary polarization by interacting with the medium together with the original driving field; this process repeats until the pulse leaves the medium. The final polarization will be temporally reshaped by this self-consistent dipole-field interaction and the short XUV pulse would develop a tail with a series of subpulses [19–23]. This temporal reshaping will affect the absorption line shape, so when we study a dense medium with ATAS, understanding macroscopic propagation effects beyond the single-atom response will become very important.

So far only a few attempts have addressed the resonant pulse propagation effects in transient absorption spectrum [24–28] or in the static absorption spectrum [29,30]. These investigations have qualitatively analyzed how the temporal and spectral reshaping evolves while an XUV pulse passes through a laser-dressed medium, yet it is still difficult to disentangle the impact of the XUV pulse reshaping and laser-induced transition on the absorption spectrum, inhibiting directly identifying fingerprints of different physical processes from the macroscopic transient absorption spectrogram.

In this article, a theoretical study of XUV absorption in the presence of a moderately intense near-infrared (NIR) pulse near the helium  $1s^2 \rightarrow 1s2p$  transition is presented. We mainly focus on two prototypical processes: One is the Rabi oscillation in a three-level system, and the other is the population transfer in a four-level system. In the case of the three-level Rabi oscillation process, apart from the normal Autler-Townes (AT) splitting in the absorption spectrum, a complex amplitude modulation on the resonance feature and a phase jump on the off-resonance feature are observed. In the calculation of the four-level population transfer process, our results show an unexpected quantum beating behavior that lasts for hundreds of femtoseconds in the case of high gas densities. An analytical expression based on a perturbative picture is deduced to interpret the connection between the absorption spectral features and the density of the gas medium. The simple analytical expression intuitively decouples contributions from different physical processes to the absorption spectrum and provides guidance on the study of optical pulse shaping and XUV molecular quantum beat spectroscopy.

\*weicao@hust.edu.cn

## II. THEORETICAL MODEL

### A. Numerically solving the time-dependent Schrödinger equation coupled with Maxwell's equations

The macroscopic transient absorption spectrum is simulated by coupling the time-dependent Schrödinger equation (TDSE) with Maxwell's equations [24]. The polarization of a single atom in the presence of laser fields is calculated from TDSE and serves as a source term for Maxwell's equation propagation. Assuming that the pulse propagates in the  $z$  direction, then a one-dimensional wave equation describing the pulse spectrum  $\tilde{E}(\omega, z, \tau)$  can be approximated by [31]

$$\frac{\partial}{\partial z} \tilde{E}(\omega, z, \tau) = -i\omega \frac{2\pi}{c} \tilde{P}(\omega, z, \tau). \quad (1)$$

The atomic response to the attosecond and femtosecond pulses is described by the wave function  $|\psi\rangle$ , and the polarization  $P(t, z, \tau)$  can be obtained by solving the TDSE:

$$i \frac{\partial}{\partial t} |\psi\rangle = \hat{H} |\psi\rangle. \quad (2)$$

The Hamiltonian  $\hat{H}$  is defined as  $\hat{H} = \hat{H}_0 + E(t, z, \tau)\hat{z}$ , where  $\hat{H}_0$  is the unperturbed Hamiltonian and the entire incident electric field  $E(t, z, \tau)$  is the sum of pump field  $E_{\text{XUV}}(t, z)$  and the time-delayed probe field  $E_{\text{IR}}(t, \tau)$ . The time domain polarization is given by

$$P(t, z, \tau) = N \times [\langle \psi | \hat{\mu} | \psi \rangle], \quad (3)$$

where  $N$  is the atomic number density and  $\hat{\mu}$  is the dipole matrix operator. The Fourier transformation of Eq. (3) gives the frequency domain polarization  $\tilde{P}(\omega, z, \tau) = \frac{1}{\sqrt{2\pi}} \int_{-\infty}^{+\infty} P(t, z, \tau) e^{-i\omega t} dt$ . The pulse spectrum  $\tilde{E}(\omega, z, \tau)$  can be obtained by solving Eqs. (1)–(3) numerically.

Then the optical density (OD) is calculated as

$$\text{OD}(\omega, z, \tau) = -\log_{10} \left| \frac{\tilde{E}(\omega, z, \tau)}{\tilde{E}(\omega, 0, \tau)} \right|. \quad (4)$$

Atomic units are used throughout. The OD values are convoluted with a Gaussian function with a linewidth of 20 meV to account for the instrumental resolution.

### B. Polarization model and analytical expression of optical density

The above full numerical treatment of the macroscopic transient absorption for long-lived states can be further restricted when the computations are too demanding. Thus a model formula for calculating the polarization response is also developed.

According to first-order perturbation theory, how the population of any state  $|n\rangle$  changes along with time can be approximated as

$$c_n(t, z, \tau) = -i \int_{-\infty}^t E(t, z, \tau) d_{ng} e^{-iE_{gn}t_1} dt_1 + \alpha(z, \tau) M_{\text{IR}}(t, \tau), \quad (5)$$

where the first term represents the time evolution of state  $|n\rangle$  caused by the XUV pulse before the arrival of the NIR pulse.

When the NIR pulse arrives, it perturbs the atomic system and changes the amplitudes and phases of  $c_n$ , which are described by the second term of Eq. (5) (here, for convenience of calculation, the NIR pulse is fixed at  $t = 0$ ).  $\alpha$  is the complex amplitude of  $c_n$  just before the NIR arrives ( $t = 0$ ) and can be calculated according to Eqs. (1) and (A5):

$$\mathcal{C}[\alpha(z, \tau)] = -\frac{1}{\sqrt{2\pi}} \int_0^\infty \frac{\chi(\omega)}{Nd_{ng}} \tilde{E}(\omega, z = 0, \tau) e^{-\frac{i2\pi\omega}{c}\chi z} d\omega. \quad (6)$$

The symbol  $\mathcal{C}$  represents the complex conjugate.  $M_{\text{IR}}(t, \tau)$  quantifies the population changes caused by the NIR pulse; it has different forms for different systems. For example,  $M_{\text{IR}}(t, \tau)$  can be written as a cosine function in a three-level Rabi oscillation system, depicting the population flopping between the two states resonantly coupled by the NIR field. If the NIR pulse width is not considered, which can be regarded as a delta pulse, then  $M_{\text{IR}}(t, \tau)$  can be represented by a Heaviside function, indicating a prompt population change induced by the NIR pulse.

Then an expression for the frequency-dependent polarization can be derived according to Eq. (5) (see Appendixes A and B for a detailed derivation):

$$\tilde{P}_n(\omega, z, \tau) = \chi(\omega) \tilde{E}(\omega, z, \tau) + \frac{i\chi(\omega) \mathcal{C}[\alpha(z, \tau)]}{\sqrt{2\pi} d_{ng}} F_{\text{IR}}(\omega, \tau). \quad (7)$$

Here, Eq. (7) has a similar form as Ref. [24] which is derived from the density matrix theory assuming a zero-duration NIR pulse.  $F_{\text{IR}}(\omega, \tau)$  is the Fourier transform of  $\frac{dM_{\text{IR}}(t)}{dt}$ , and its specific form for different processes is given in Appendixes A and B. The susceptibility  $\chi(\omega)$  is

$$\chi(\omega) = \frac{-Nd_{ng}^2}{\omega - E_{ng} - i\gamma_n}, \quad (8)$$

where  $E_{ng}$  and  $d_{ng}$  represent the energy difference and dipole matrix element between the excited state  $|n\rangle$  and the ground state  $|g\rangle$ , respectively.  $\gamma_n$  is the lifetime of the excited state  $|n\rangle$ .

With the help of Eqs. (1) and (7), the absorbance can be calculated. Although the analytical formula of the polarization in Eq. (7) speeds up the modeling of the macroscopic effect to a great extent, it is still difficult to gain insight into the physical processes that lead to the complex absorption spectrum, especially how to pinpoint the effects of the XUV and NIR pulses. Thus, by substituting Eq. (7) into Eq. (1), an analytical expression for the absorption spectrum is further deduced to explore the origins of macroscopic signatures in a quantitative way (see Appendix C):

$$\text{OD}(\omega, z, \tau) = -\log_{10} \left[ e^{\frac{4\pi\omega z}{c} \text{Im}(\chi)} \{1 + |H_1(\omega, z, \tau)|^2 + 2 \text{Re}[H_1(\omega, z, \tau)]\} \right]. \quad (9)$$

Equation (9) is the main result of this work. There are three terms in Eq. (9) and each term has a specific physical significance. The first term  $e^{\frac{4\pi\omega z}{c} \text{Im}(\chi)}$  is the XUV

propagation term in the absence of the NIR pulse, and the absorption spectrum has a typical Lorentzian line shape. The integral  $H_1(\omega, z, \tau) = \frac{A(\omega)B(\omega, \tau)}{E(\omega, 0, \tau)} \int_0^z \mathcal{C}[\alpha(z_1, \tau)] e^{iA(\omega)z_1} dz_1$  appearing in both the second and third terms represents the coupling strength of the NIR and XUV pulse, where  $A(\omega) = \frac{2\pi\omega\chi}{c}$ ,  $B(\omega, \tau) = \frac{F_{\text{IR}}(\omega, \tau)}{\sqrt{2\pi}d_{ng}}$ . The information on the NIR pulse is associated with parameter  $B$ , while the XUV pulse information is imprinted in  $\mathcal{C}[\alpha(z, \tau)]$ . If  $H_1$  is much smaller than unity, then the second term  $|H_1|^2$ , which is the modulus square of  $H_1$ , can be considered as a small quantity. In this case the third term  $2\text{Re}(H_1)$ , which scales linearly with  $\alpha$ , is dominant. Conversely, if the value of the coupling term  $H_1$  is very large, then the second term will be dominant over the third term. Since  $H_1$  is proportional to the susceptibility  $\chi(\omega)$ , the second term will normally dominate the near-resonant absorption features and the third term dominates the off-resonant absorption features. In the following section, we will apply these general principles embodied in Eq. (9) to inspect the macroscopic signatures of a few spectroscopic features.

### III. RESULTS AND DISCUSSION

In this section, we mainly study two basic scenarios in attosecond XUV transient absorption measurements, the AT splitting and quantum beating effect, which is performed by studying a three-level system and then a four-level system, respectively. When the propagation effect is considered, these two effects will appear in the absorption spectrum as complex spectral profiles. How to analyze this complex absorption spectrum is the key to understanding the propagation effect and other nonlinear effects. Equation (9) can be regarded as a bridge to deal with this problem.

#### A. Macroscopic effects on AT splitting

Figure 1(a) shows the energy diagram of a three-level system interacting with a resonant laser pulse. A ground state  $1s^2$  (0 eV) and two excited states  $1s2p$  (21.2 eV) and  $1s3s$  (22.9 eV) are included in our calculation. The dipole matrix elements are  $d_{12} = 0.42$ ,  $d_{23} = 1.87$  [24]. The atomic system is exposed to a weak XUV pulse with a peak intensity of  $1 \times 10^{10}$  W/cm<sup>2</sup>, a pulse duration of 230 attoseconds (as), and a photon energy of 21.2 eV. The strong NIR pulse with a peak intensity of  $1 \times 10^{13}$  W/cm<sup>2</sup>, a central wavelength of 730 nm, and a pulse duration of 5 fs, is resonant with the transition between the  $1s2p$  and  $1s3s$  states. Both pulses have initial Gaussian profiles in the time domain and the NIR pulse is delayed by  $\tau$  with respect to the XUV pulse centered at  $t = 0$ . Positive delay indicates that the NIR pulse arrives after the XUV pulse.

Figures 1(b) and 1(c) are transient absorption spectra in the vicinity of the  $1s2p$  resonance energy at two different atomic densities by numerically solving the TDSE coupled with Maxwell's wave equation. The typical AT splitting feature corresponds to the bifurcation of the energy level at 21.2 eV. Figure 1(b) corresponds to the single-atom response calculated at a pressure of 0.0001 Torr with a propagation length  $z = 2 \mu\text{m}$ . The spacing between the two symmetrically split energy levels is  $\Omega_R$  in Fig. 1(b) at around zero delay,

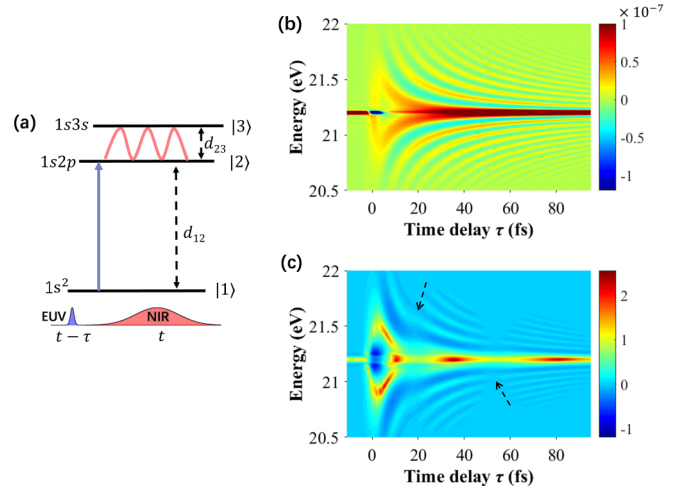


FIG. 1. (a) Energy diagram of a three-level system of helium atoms interacting with the XUV-NIR pulse sequence. The transient absorption spectrum in the vicinity of the  $1s2p$  resonance energy is calculated at a pressure of 0.0001 Torr with a propagation length  $z = 2 \mu\text{m}$  (b) and a pressure of 50 Torr with a propagation length  $z = 200 \mu\text{m}$  (c) in our numerical calculations.

where  $\Omega_R = \sqrt{|d_{23}|^2 E_0^2}$  is the Rabi frequency ( $E_0$  is the peak intensity of the NIR electric field; here,  $E_0 = 0.0168$ ,  $\Omega_R = 0.85$  eV). It has been extensively studied [32–35] in a single-atom response, and we will not discuss it here specifically. We mainly focus on the study of the macroscopic absorption spectrum in Fig. 1(c) calculated at a pressure of 50 Torr with a propagation length  $z = 200 \mu\text{m}$ . After considering the propagation effect, more complex and richer absorption structures emerge: In addition to the similar symmetric splitting of energy levels as in a single-atom response, a strong-weak alternating absorption at 21.2 eV, and hyperbolic lines experiencing abrupt bending or phase jumps at certain time delays [i.e., 20 and 55 fs as indicated by the dashed arrows in Fig. 1(c)] are observed. Further calculations show that the absorption profile is tunable by adjusting parameters such as the density of gas, and the intensity and the wavelength of the NIR pulse, which is of great significance to the study of XUV optical pulse shaping [36].

Before applying Eq. (9) to explain the complex absorption structures in Fig. 1(c), we first compare the absorption spectrum obtained by the numerical simulation, the polarization spectrum of Eq. (9). Figures 2(a) and 2(b) show a comparison between a full simulation based on Eqs. (1)–(3) and the model calculation using Eqs. (7) and (1). The same features are captured by using the model approximation in macroscopic propagation. By comparing the absorption spectrum calculated by the analytical expression of Eq. (9) [Fig. 2(c)] with the model calculation based on Eq. (7) [Fig. 2(b)], it is found that the sideband structure and absorption characteristic at the 21.2 eV resonance center are also well reproduced. All of them are calculated using the same parameters as Fig. 1(c). It should be noted that Eq. (7) is derived assuming that the NIR pulse arrives after the XUV pulse, therefore Eqs. (7) and (9) will no longer be applicable when the delay is close to

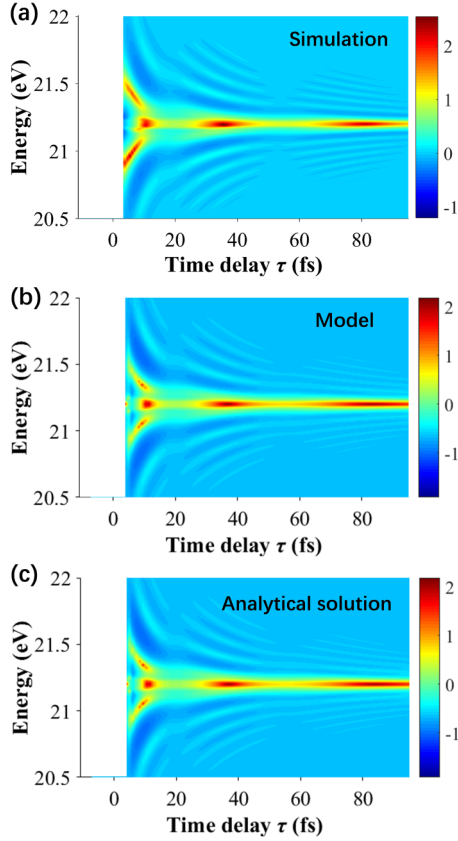


FIG. 2. Comparison of transient absorption spectra in the vicinity of the  $1s2p$  resonance energy calculated with different methods. (a) is a full numerical simulation based on Eqs. (1)–(3), (b) is the model calculation with Eq. (7), and (c) is the analytical solution of Eq. (9). The parameters are the same as in Fig. 1(c).

zero considering a finite pulse duration of the NIR pulse. In order to circumvent this issue, we block out the results for delays of less than 10 fs in Fig. 2. The excellent agreement between the results in Fig. 2 confirms the validity of the analytical solution in Eq. (9).

According to Eq. (9), a complex absorption spectrum can be broken down into three parts. The results of the analysis for each term of Eq. (9) are shown in Fig. 3. Figure 3(a) shows the absorption spectrum obtained by considering only the first term. It has a delay-independent Lorentzian line profile, which is mainly caused by the XUV-induced free induction decay and obeys Beer's law in case of a dilute-gas medium [17]. Figure 3(b) shows the absorption profile attributed to the second term of Eq. (9); it reveals the near-resonant absorption features (around 21.2 eV) of an XUV pulse propagating through an optically dense medium. The delay-dependent modulation of the absorption is determined by the coupling coefficient  $H_1$  shown in Fig. 3(d). The nonperiodic modulation in OD is a typical result of the interplay between the radiating dipole and the incident light in a dense medium and has been studied in both optical and XUV regimes [24–30]. The calculation shows that this modulation solely follows the delay-dependent quantity of  $\mathcal{C}[\alpha(\tau)]$ , confirming that the absorption at the resonance energy of 21.2 eV is only associated with the propagation effect of the XUV pulse. For the off-resonance absorption

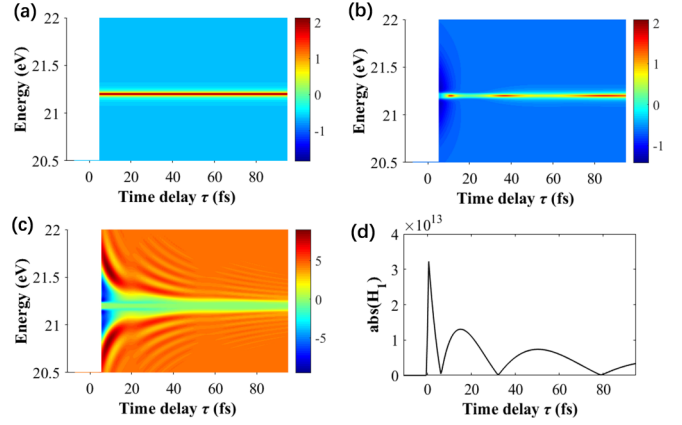


FIG. 3. OD spectrum calculated with Eq. (9) ( $z = 200 \mu\text{m}$  propagation length and a gas pressure of 50 Torr) with only the first term (a) or second term (b) included. (c) is  $2 \text{Re}(H_1)$ , the third term in Eq. (9). The corresponding absolute value of the parameter  $H_1$  [Eq. (9)] at 21.2 eV is shown in (d), where  $A = \frac{2\pi\omega\chi}{c}$ ,  $B = \frac{R_b d_{nk}}{d_{ng}}$  (see Appendix A for a detailed derivation).

features, since the susceptibility  $\chi(\omega)$  decreases rapidly,  $H_1$  becomes a rather small quantity and the absorption profile is mainly determined by the third term of Eq. (9). In case of a laser-driven Rabi-cycling process as shown in Fig. 1,  $R_b(\omega)$ , which represents the Fourier transform of the Rabi oscillation, bifurcates about the resonant position (21.2 eV) and contributes significantly to the off-resonance features. Therefore, the NIR pulse's effect is mainly imprinted in the off-resonance structure in the absorption spectrum. The interplay between  $R_b$  associated with the NIR pulse and  $\mathcal{C}[\alpha(\tau)]$  associated with the XUV pulse gives rise to the complex hyperbolic absorption features as shown in Fig. 3(c). Thus the absorption caused by different physical mechanisms can be quantified separately through Eq. (9), which provides great convenience for the study of a complex macroscopic absorption spectrum.

### B. Macroscopic effects on quantum beats

Next, we apply Eq. (9) to investigate the electronic quantum beating effect in attosecond transient absorption. A typical quantum beat process is closely related to the population transfer via a two-photon transition, as shown in Fig. 4(a). The dark state  $1s3s$  (22.9 eV) serves as the near-resonant intermediate state. The NIR pulse with a central wavelength of 1326 nm assists population transfer from the bright  $1s3p$  (23.09 eV) state to the other bright state  $1s2p$  (21.2 eV), and the interference between the three-photon and one-photon pathway leads to oscillating features in the absorption spectrum (i.e., the quantum beat signature), which has been widely studied in the single-atom response [3,7,8,32,37–39]. Figures 4(b) and 4(c) are the transient absorption spectra that are numerically simulated based on Eqs. (1)–(3) in the vicinity of the  $1s2p$  resonance energy. The quantum beat clearly appears in both the single-atom response [Fig. 4(b)] and macroscopic gas medium [Fig. 4(c)]. The simulation shows that the modulation of OD at the vicinity of the resonance is enhanced and lasts longer in the case of a dense gas medium; the time duration of the beating behavior in Fig. 4(b) ends at about

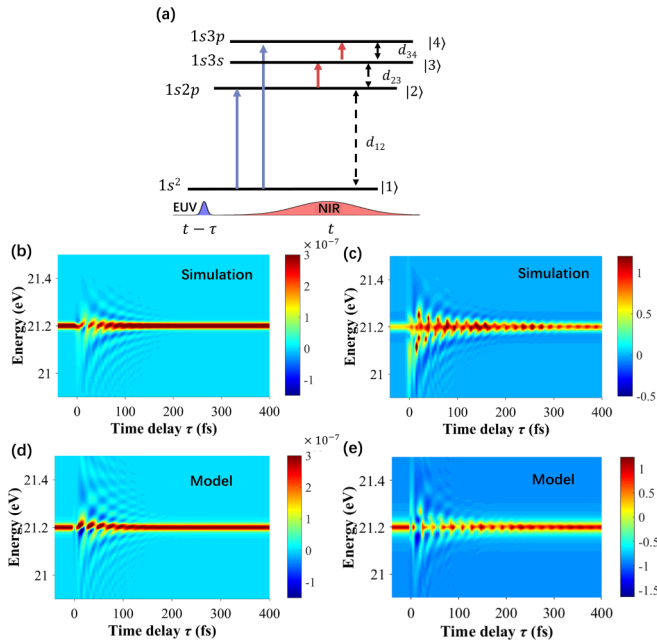


FIG. 4. (a) Energy diagram for a four-level helium atom interacting with XUV and NIR pulses. (b) and (c) are the transient absorption spectra on two different color scales simulated based on Eqs. (1)–(3) in the vicinity of the  $1s2p$  resonance energy, which has the same parameters as Fig. 1, that the dressing field is a two-cycle, 1326-nm pulse with a peak intensity of  $1 \times 10^{12}$  W/cm<sup>2</sup>. The corresponding model results of the single-atom response (d) and macroscopic propagation (e) are calculated with Eq. (7) combined with Eq. (1).

150 fs while in Fig. 4(c) the beating extends beyond 400 fs. Such a lengthening of the time of the quantum beat caused by the macroscopic effect is of great significance to the study of molecular quantum beat spectra. Recently, the vibrational quantum beats with a fundamental period of 50 fs persisting for a picosecond are observed in the  $b^1\Sigma_u^+$  valence state of molecular nitrogen using attosecond transient absorption spectroscopy [40]; such a long-lasting quantum beat signal is necessary to distinguish vibrational levels in molecules since the spacing between adjacent vibrational levels is very small. Therefore, molecular time-domain spectroscopies may benefit from an optically dense medium where the macroscopic effect is playing a role.

Now we turn to Eq. (9) to interpret the persisting quantum beating behavior caused by the macroscopic effect. Figures 4(d) and 4(e) show the model calculation using Eqs. (7) and (1), where  $F_{\text{IR}} = 1 - \mathcal{C}[L(\tau)]$  (see Appendix B for a detailed derivation), and the same oscillation features are captured by the model calculation, not only in the single-atom response but also in macroscopic propagation, indicating again the validity of Eq. (7) and the analytical solution derived from it.

Figure 5(a) shows the macroscopic absorption spectrum versus time calculated with Eq. (9); the oscillating features are also well reproduced. For the absorption spectrum corresponding to the macroscopic quantum beating effect, the resonant absorption feature and the off-resonance absorption features can still be separated to analyze the macroscopic absorption spectra similar to Fig. 3. The calculational result

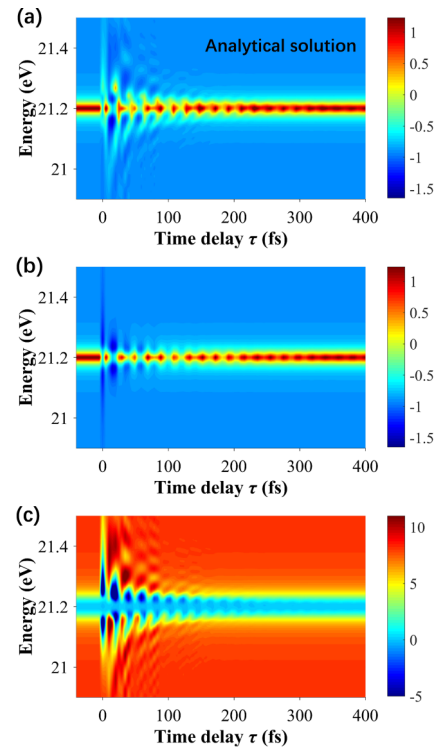


FIG. 5. OD spectrum in the vicinity of the  $1s2p$  resonance calculated with Eq. (9) ( $z = 200 \mu\text{m}$  propagation length and a gas pressure of 50 Torr) with only the first term (a) or second term (b) included. (c) is  $2\text{Re}(H_1)$ , the third term in Eq. (9). The laser parameters are the same as in Fig. 4.

of the second term is shown in Fig. 5(b), which mainly contributes to the signal at the resonance center of 21.2 eV, and the calculational result of the third term is shown in Fig. 5(c), which dominates the absorption signal away from the resonance.

The persisting oscillation characteristics we pay attention to are mainly residing in the near-resonance feature shown in Fig. 5(b). It can be understood in a quantitative way by analyzing the integral  $H_1 = \frac{AB}{E(\omega, 0, \tau)} \int_0^z \mathcal{C}[\alpha(z_1, \tau)] e^{iAz_1} dz_1$  appearing both in the second term and third term. In the case of macroscopic absorption, for the parameters used in our simulation (i.e.,  $z = 200 \mu\text{m}$  propagation length and a gas pressure of 50 Torr), the integral  $\int_0^z \mathcal{C}[\alpha(z_1, \tau)] e^{iAz_1} dz_1$  is a large quantity, and the absolute value of  $H_1$  is on the order of  $10^{22}$  as shown in Fig. 6(b), so the second term, which is mainly localized around the resonance center, is dominant. The absorption around the resonance center results from the interplay between the XUV pulse propagation and the NIR-induced population transfer process. This is different from the case of AT splitting, where the resonance absorption is only determined by the XUV pulse propagation. For the single-atom response, the integral  $\int_0^z \mathcal{C}[\alpha(z_1, \tau)] e^{iAz_1} dz_1$  is a small quantity, and the absolute value of  $H_1$  is on the order of  $10^{-6}$  as shown in Fig. 6(a), so the third term, which represents the absorption away from the resonance center, is dominant. The above analysis shows that when noticeable population transfer occurs in an optically dense medium, the absorption feature is mainly determined by the second term of Eq. (9),

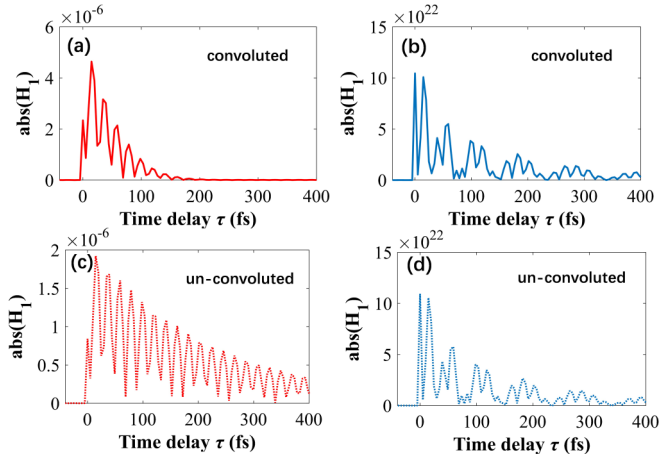


FIG. 6. The absolute value of coupling strength  $H_1$  at 21.2 eV, as a function of the delay  $\tau$  in the single-atom response [(a), (c)] and in the macroscopic gas medium [(b), (d)]. Here,  $A = \frac{2\pi\omega\chi}{c}$ ,  $B = \frac{1-\mathcal{C}(L)}{\sqrt{2\pi d_{ng}}}$ . (a) and (b) are the results convoluted with a Gaussian linewidth function of 20 meV, while (c) and (d) are the unconvoluted results.

while in the case of a dilute gas, the third term starts to dominate the absorption spectrum that mimics the single-atom response.

In the OD calculation throughout this article, the simulated spectra are convoluted with a Gaussian function with a linewidth of 20 meV to account for the instrumental resolution. The convolution operator coherently adds up the nearby oscillatory features around a resonant energy [41]. The beating frequency at the resonance center (21.2 eV) is slightly different from that at nearby transition energies due to the hyperbolic line profiles. For the single-atom response, the absorption spectrum has a broad feature as indicated by Fig. 5(c). The convolution operator adds signals with slightly different oscillating periods coherently within the 20 meV band, and forms a time-domain wave packet that is much shorter than the coherence time of the single oscillating energy component. This is equivalent to artificially adding a fast decaying factor on the radiation dipole [42], and explains the earlier termination of the quantum beat feature in Fig. 4(b). However, the rapid oscillation persists for a much longer time even after convolution in the case of macroscopic absorption. This is due to the fact that only the frequency component at the resonance center is contributing to the absorption profile according to the second term in Eq. (9), and the beating time is determined by the coherence time of the radiation dipole, which is over 500 fs in our simulation.

In order to better compare the influence of instrument resolution on absorption spectrum, we also calculate the coupling term  $H_1$  with and without considering the instrument resolution, as shown in Fig. 6. In the case of the single-atom response, the oscillation decays much faster when the instrumental resolution is considered as shown in Figs. 6(a) and 6(c). However, the decaying constant of the oscillation is hardly affected by the instrument resolution in the case of an optically dense target as shown in Figs. 6(b) and 6(d). Therefore, in order to observe relatively fine spectral structures that require very high resolution in a time-resolved spectroscopic

measurement, the propagation effect needs to be properly considered.

#### IV. CONCLUSION

In summary, the transient XUV absorption spectroscopy for an optically dense medium is investigated. An analytical expression is derived for explaining some new absorption properties in macroscopic absorption. By using the analytical expression, a complex absorption spectrum can be divided into three parts: a delay-independent term that is solely determined by the XUV-induced free induction decay, a cross term that scales linearly with the coupling strength  $H_1(\tau)$  depicting the interplay between XUV and NIR pulses, and a third term that scales quadratically with the coupling strength and mainly gives rise to the localized absorption feature around the resonance energy.

The analytical expression is applied to inspect two prototypical scenarios: a Rabi oscillation process in a three-level system where the NIR pulse width is considered and the population transfer process in a four-level system where the NIR pulse width is neglected. The complex spectral splitting occurring for the three-level system as well as the long persisting oscillation for the four-level system in a macroscopic absorption spectrum is well explained, and the underlying physical origins of these macroscopic signatures are successfully pinpointed. It should be noted that the application of the analytical expression of optical density is not limited to the two prototypical spectroscopic features discussed in this article. As long as the NIR pulse is short as compared to the lifetime of the involved excited state, and the NIR-induced population change function  $M_{IR}(t, \tau)$  is known [the analytical form of  $M_{IR}(t, \tau)$  is accessible for the two special cases discussed in this article; for more complex cases  $M_{IR}(t, \tau)$  can be calculated numerically for a single-atom response], it can be extended to more general cases of laser-matter interaction.

The current study provides a simple and intuitive approach for understanding transient absorption spectroscopies in an optically dense medium. It also offers an effective guidance for exploring applications such as optical pulse shaping and time-resolved spectroscopies for systems with congested energy levels.

#### ACKNOWLEDGMENTS

We acknowledge Stephen Leone for helpful discussions. This research was supported by the National Natural Science Foundation of China under Grant No. 12021004, and National Key Research and Development Program under Grant No. 2017YFE0116600.

#### APPENDIX A: THREE-LEVEL RABI OSCILLATION MODEL

In a three-level Rabi oscillation system, the NIR pulse has a finite pulse duration and causes periodic inversion of particle numbers between bright and dark states, it can be approximately represented by a cosine function  $\cos[\Omega(t)]$ , where  $\Omega(t)$  is the area of NIR pulse. Then Eq. (5) can be

expressed as

$$c_n(t, z, \tau) = -i \int_{-\infty}^t E(t_1, z, \tau) d_{ng} e^{-iE_{gn}t_1} dt_1 + \alpha(z, \tau) \{\cos[\Omega(t)] - 1\}, \quad (\text{A1})$$

where  $\Omega(t) = \frac{E_0}{2} d_{nk} \int_{-\infty}^t e^{-t_1^2/T_0^2} dt_1$ ,  $E_0$  is the peak intensity of the NIR electric field,  $T_0$  represents the pulse width of NIR, and  $d_{nk}$  represents the dipole matrix element between bright and dark states.  $\tilde{c}_n(\omega, z, \tau)$  is obtained by taking the derivative of both sides of Eq. (A1) first:

$$c'_n(t, z, \tau) = -iE(t, z, \tau) d_{ng} e^{-iE_{gn}t} - \alpha(z, \tau) \frac{E_0}{2} d_{nk} \sin[\Omega(t)] e^{-t^2/T_0^2}. \quad (\text{A2})$$

Then take the Fourier transform of both sides of Eq. (A2),

$$\tilde{c}_n(\omega, z, \tau) = \frac{-i\tilde{E}(\omega + E_{gn}, z, \tau) d_{ng}}{i\omega} - \frac{\alpha(z, \tau) d_{nk} R_b(\omega)}{i\omega}, \quad (\text{A3})$$

where  $R_b(\omega) = \frac{E_0}{2\sqrt{2\pi}} \int_{-\infty}^{+\infty} \sin[\Omega(t)] e^{-t^2/T_0^2} \cdot e^{-i\omega t} dt$  represents the frequency-dependent Rabi-oscillation term.

Consider the dipole moment formed by the coherence between the ground state  $|g\rangle$  and the excited state  $|n\rangle$ . The wave function can be written as follows:

$$|\psi\rangle = e^{-iE_g t} |g\rangle + c_n(t) e^{-iE_n t} |n\rangle. \quad (\text{A4})$$

Then the dipole moment  $D_n(t, z, \tau)$  is defined as

$$D_n(t, z, \tau) = \langle \psi | r | \psi \rangle = \mathcal{C}[c_n(t, z, \tau)] d_{ng} e^{iE_{ng}t} + c_n(t, z, \tau) d_{ng} e^{-iE_{ng}t}. \quad (\text{A5})$$

Since  $E_{ng}$  is in the XUV region, the first term in Eq. (A5) represents the positive frequency components and the first term represents the negative frequency components. Only the positive frequency is meaningful and will be considered in the following derivation. Therefore, the Fourier transform of Eq. (A5) gives

$$\begin{aligned} \tilde{D}_n(\omega, z, \tau) &= \frac{1}{\sqrt{2\pi}} \int_{-\infty}^{+\infty} \mathcal{C}[c_n(t, z, \tau)] d_{ng} e^{iE_{ng}t} e^{-i\omega t} dt \\ &= \mathcal{C}[\tilde{c}_n(-\omega + E_{ng}, z, \tau)] d_{ng} \\ &= \frac{\tilde{E}(\omega, z, \tau) d_{ng}^2}{\omega - E_{ng}} - \frac{d_{nk} d_{ng} \mathcal{C}[\alpha(z, \tau)] R_b(\omega - E_{ng})}{i(\omega - E_{ng})} \end{aligned} \quad (\text{A6})$$

(for the real-valued electric field,  $\tilde{E}(\omega, z, \tau) = \mathcal{C}[\tilde{E}(-\omega, z, \tau)]$ ). Where  $E_{ng} = E_n + i\gamma_n$  specifies the energy range between the excited state  $|n\rangle$  and ground state  $|g\rangle$ , it depends on the energy level  $E_n$  and the lifetime  $\gamma_n$  of the excited state ( $\gamma_{2p} = 5$  meV in this article). Then the frequency-dependent polarization can be derived,

$$\begin{aligned} \tilde{P}_n(\omega, z, \tau) &= -N \tilde{D}_n(\omega, z, \tau) = N \left[ \frac{-\tilde{E}(\omega, z, \tau) d_{ng}^2}{\omega - E_n - i\gamma_n} + \frac{d_{nk} d_{ng} \mathcal{C}[\alpha(z, \tau)] R_b(\omega - E_{ng})}{i(\omega - E_n - i\gamma_n)} \right] \\ &= \chi(\omega) \tilde{E}(\omega, z, \tau) + i\chi(\omega) \mathcal{C}[\alpha(z, \tau)] R_b(\omega - E_{ng}) \frac{d_{nk}}{d_{ng}} = \chi(\omega) \tilde{E}(\omega, z, \tau) + \frac{i\chi(\omega) \mathcal{C}[\alpha(z, \tau)]}{\sqrt{2\pi} d_{ng}} (\sqrt{2\pi} R_b d_{nk}) \\ &= \chi(\omega) \tilde{E}(\omega, z, \tau) + \frac{i\chi(\omega) \mathcal{C}[\alpha(z, \tau)]}{\sqrt{2\pi} d_{ng}} F_{\text{IR}}(\omega), \end{aligned} \quad (\text{A7})$$

where  $F_{\text{IR}} = \sqrt{2\pi} d_{nk} R_b(\omega - E_{ng})$  refers to the modification induced by the NIR field to the polarization.

## APPENDIX B: FOUR-LEVEL POPULATION TRANSFER MODEL

In a four-level population transfer system, if the NIR pulse width is not considered, it can be represented by a Heaviside function  $S(t)$ . Then Eq. (5) can be expressed as

$$c_n(t, z, \tau) = -i \int_{-\infty}^t E(t_1, z, \tau) d_{ng} e^{-iE_{gn}t_1} dt_1 + \alpha(z, \tau) S(t) [L(\tau) - 1]. \quad (\text{B1})$$

Then  $\tilde{c}_n(\omega, z, \tau)$  is obtained by taking the derivative and Fourier transform to Eq. (B1) as follows,

$$c'_n(t, z, \tau) = -iE(t, z, \tau) d_{ng} e^{-iE_{gn}t} + \alpha(z, \tau) \delta(t) [L(\tau) - 1], \\ i\omega \tilde{c}_n(\omega, z, \tau) = -i\tilde{E}(\omega + E_{gn}, z, \tau) d_{ng} + \frac{\alpha(z, \tau) [L(\tau) - 1]}{\sqrt{2\pi}},$$

$$\tilde{c}_n(\omega, z, \tau) = \frac{-i\tilde{E}(\omega + E_{gn}, z, \tau) d_{ng}}{i\omega} + \frac{\alpha(z, \tau) [L(\tau) - 1]}{i\omega \sqrt{2\pi}}, \quad (\text{B2})$$

where  $L(\tau)$  refers to the modification induced by the NIR field to the polarization. What is different from the three energy levels discussed above is that, not only should we consider the coupling process between bright and dark states occurring in the three energy levels, but also the coupling process of coherent excited states, so a dipole-control model [18,29,43,44] is used in the calculation of four energy levels, which contains both processes entirely:

$$L(\tau) = a_1 e^{i\phi_1} + a_2 e^{i\Delta\omega(-\tau) + i\phi_2}. \quad (\text{B3})$$

$a_1, a_2, \phi_1, \phi_2$  represent the amplitude and phase parameters, which quantify the value of coherences between the ground and excited states after the interaction with the NIR pulse. Here, the full form  $\mathcal{C}[L(\tau)] = 0.36e^{i(0.27\pi)} + e^{-i(1.87\tau) + i(1.13\pi)}$  is used in our calculation to match the numerical results.

Substitute  $\tilde{c}_n(\omega, z, \tau)$  in Eq. (B2) into the expression for the dipole moment,

$$\begin{aligned} \tilde{D}_n(\omega, z, \tau) &= \mathcal{C}[\tilde{c}_n(-\omega + E_{ng}, z, \tau)]d_{ng} \\ &= \frac{\tilde{E}(\omega, z, \tau)d_{ng}^2}{\omega - E_{ng}} + \frac{\mathcal{C}[\alpha(z, \tau)(L(\tau) - 1)]d_{ng}}{i(\omega - E_{ng})\sqrt{2\pi}}. \end{aligned} \quad (\text{B4})$$

Then the frequency-dependent polarization can be derived:

$$\begin{aligned} \tilde{P}_n(\omega, z, \tau) &= -N\tilde{D}_n(\omega, z, \tau) = N \left[ \frac{-\tilde{E}(\omega, z, \tau)d_{ng}^2}{\omega - E_n - i\gamma_n} \right. \\ &\quad \left. - \frac{\mathcal{C}\{\alpha(z, \tau)[L(\tau) - 1]\}d_{ng}}{i(\omega - E_n - i\gamma_n)\sqrt{2\pi}} \right] \\ &= \chi(\omega)\tilde{E}(\omega, z, \tau) \\ &\quad + \frac{i\chi(\omega)\mathcal{C}[\alpha(z, \tau)]}{\sqrt{2\pi}d_{ng}} \{1 - \mathcal{C}[L(\tau)]\} \\ &= \chi(\omega)\tilde{E}(\omega, z, \tau) + \frac{i\chi(\omega)\mathcal{C}[\alpha(z, \tau)]}{\sqrt{2\pi}d_{ng}} F_{\text{IR}}(\tau). \end{aligned} \quad (\text{B5})$$

Here,  $F_{\text{IR}} = 1 - \mathcal{C}[L(\tau)]$  refers to the modification induced by the NIR field to the polarization.

### APPENDIX C: ANALYTICAL EXPRESSION OF ABSORPTION SPECTRUM

By substituting Eq. (7) into Eq. (1),

$$\begin{aligned} \frac{\partial}{\partial z} \tilde{E}(\omega, z, \tau) &= -i \frac{2\pi\omega\chi}{c} \tilde{E}(\omega, z, \tau) \\ &\quad + \frac{2\pi\omega\chi}{c} \frac{F_{\text{IR}}(\omega, \tau)}{\sqrt{2\pi}d_{ng}} \mathcal{C}[\alpha(z, \tau)], \end{aligned} \quad (\text{C1})$$

where  $\frac{2\pi\omega\chi}{c} = A(\omega)$ ,  $\frac{F_{\text{IR}}(\omega, \tau)}{\sqrt{2\pi}d_{ng}} = B(\omega, \tau)$ , Eq. (C1) is further written as follows:

$$\begin{aligned} \frac{\partial}{\partial z} \tilde{E}(\omega, z, \tau) &= -iA(\omega)\tilde{E}(\omega, z, \tau) \\ &\quad + A(\omega)B(\omega, \tau)\mathcal{C}[\alpha(z, \tau)]. \end{aligned} \quad (\text{C2})$$

$\tilde{E}(\omega, z, \tau)$  can be derived from Eq. (C2):

$$\begin{aligned} \tilde{E}(\omega, z, \tau) &= \tilde{E}(\omega, 0, \tau)e^{-iA(\omega)z} + e^{-iA(\omega)z} \\ &\quad \times \int_0^z A(\omega)B(\omega, \tau)\mathcal{C}[\alpha(z_1, \tau)]e^{iA(\omega)z_1} dz_1. \end{aligned} \quad (\text{C3})$$

By substituting Eq. (C3) into Eq. (4),

$$\begin{aligned} \text{OD}(\omega, z, \tau) &= -\log_{10} \left| \frac{\tilde{E}(\omega, z, \tau)}{\tilde{E}(\omega, 0, \tau)} \right|^2 = -\log_{10} \left| \frac{\tilde{E}(\omega, 0, \tau)e^{-iAz} + e^{-iAz}AB \int_0^z \mathcal{C}[\alpha(z_1, \tau)]e^{iAz_1} dz_1}{\tilde{E}(\omega, 0, \tau)} \right|^2 \\ &= -\log_{10} \left| e^{-i\frac{2\pi\omega\chi}{c}z} + e^{-i\frac{2\pi\omega\chi}{c}z} \frac{AB}{\tilde{E}(\omega, 0, \tau)} \int_0^z \mathcal{C}[\alpha(z_1, \tau)]e^{iAz_1} dz_1 \right|^2 \\ &= -\log_{10} \left[ e^{\frac{4\pi\omega z}{c} \text{Im}(\chi)} + e^{\frac{4\pi\omega z}{c} \text{Im}(\chi)} \left| \frac{AB}{\tilde{E}(\omega, 0, \tau)} \int_0^z \mathcal{C}[\alpha(z_1, \tau)]e^{iAz_1} dz_1 \right|^2 \right. \\ &\quad \left. + 2e^{\frac{4\pi\omega z}{c} \text{Im}(\chi)} \text{Re} \left( \frac{AB}{\tilde{E}(\omega, 0, \tau)} \int_0^z \mathcal{C}[\alpha(z_1, \tau)]e^{iAz_1} dz_1 \right) \right] \\ &= -\log_{10} \left[ \left( e^{\frac{4\pi\omega z}{c} \text{Im}(\chi)} \right) \{1 + |H_1(\omega, z, \tau)|^2 + 2 \text{Re}[H_1(\omega, z, \tau)]\} \right]. \end{aligned} \quad (\text{C4})$$

Here,  $H_1(\omega, z, \tau) = \frac{A(\omega)B(\omega, \tau)}{\tilde{E}(\omega, 0, \tau)} \int_0^z \mathcal{C}[\alpha(z_1, \tau)]e^{iA(\omega)z_1} dz_1$  appearing in both the second and third terms represents the coupling strength of the NIR and XUV pulse.

- [1] H. Wang, M. Chini, S. Chen, C.-H. Zhang, F. He, Y. Cheng, Y. Wu, U. Thumm, and Z. Chang, Attosecond Time-Resolved Autoionization of Argon, *Phys. Rev. Lett.* **105**, 143002 (2010).
- [2] M. Chini, B. Zhao, H. Wang, Y. Cheng, S. X. Hu, and Z. Chang, Subcycle ac Stark Shift of Helium Excited States Probed with Isolated Attosecond Pulses, *Phys. Rev. Lett.* **109**, 073601 (2012).
- [3] M. Chini, X. Wang, Y. Cheng, Y. Wu, D. Zhao, D. A. Telnov, S.-I. Chu, and Z. Chang, Sub-cycle oscillations in virtual states brought to light, *Sci. Rep.* **3**, 1105 (2013).

- [4] J. E. Bækhoj, L. Yue, and L. B. Madsen, Nuclear-motion effects in attosecond transient-absorption spectroscopy of molecules, *Phys. Rev. A* **91**, 043408 (2015).
- [5] Y. Cheng, M. Chini, X. Wang, A. González-Castrillo, A. Palacios, L. Argenti, F. Martín, and Z. Chang, Reconstruction of an excited-state molecular wave packet with attosecond transient absorption spectroscopy, *Phys. Rev. A* **94**, 023403 (2016).
- [6] C.-T. Liao, X. Li, D. J. Haxton, T. N. Rescigno, R. R. Lucchese, C. W. McCurdy, and A. Sandhu, Probing autoionizing states of molecular oxygen with XUV transient absorption:

- Electronic-symmetry-dependent line shapes and laser-induced modifications, *Phys. Rev. A* **95**, 043427 (2017).
- [7] W. Cao, E. R. Warrick, D. M. Neumark, and S. R. Leone, Attosecond transient absorption of argon atoms in the vacuum ultraviolet region: line energy shifts versus coherent population transfer, *New J. Phys.* **18**, 013041 (2016).
- [8] E. R. Warrick, W. Cao, D. M. Neumark, and S. R. Leone, Probing the dynamics of Rydberg and valence states of molecular nitrogen with attosecond transient absorption spectroscopy, *J. Phys. Chem. A* **120**, 3165 (2016).
- [9] M. Schultze, E. M. Bothschafter, A. Sommer, S. Holzner, W. Schweinberger, M. Fiess, M. Hofstetter, R. Kienberger, V. Apalkov, V. S. Yakovlev *et al.*, Controlling dielectrics with the electric field of light, *Nature (London)* **493**, 75 (2013).
- [10] M. Schultze, K. Ramasesha, C. Pemmaraju, S. Sato, D. Whitmore, A. Gandman, J. S. Prell, L. J. Borja, D. Prendergast, K. Yabana, D. M. Neumark, and S. R. Leone, Attosecond band-gap dynamics in silicon, *Science* **346**, 1348 (2014).
- [11] M. Lucchini, S. A. Sato, A. Ludwig, J. Herrmann, M. Volkov, L. Kasmi, Y. Shinohara, K. Yabana, L. Gallmann, and U. Keller, Attosecond dynamical Franz-Keldysh effect in polycrystalline diamond, *Science* **353**, 916 (2016).
- [12] C.-M. Jiang, L. R. Baker, J. M. Lucas, J. Vura-Weis, A. P. Alivisatos, and S. R. Leone, Characterization of photo-induced charge transfer and hot carrier relaxation pathways in spinel cobalt oxide ( $\text{Co}_3\text{O}_4$ ), *J. Phys. Chem. C* **118**, 22774 (2014).
- [13] E. Goulielmakis, Z.-H. Loh, A. Wirth, R. Santra, N. Rohringer, V. S. Yakovlev, S. Zherebtsov, T. Pfeifer, A. M. Azzeer, M. F. Kling *et al.*, Real-time observation of valence electron motion, *Nature (London)* **466**, 739 (2010).
- [14] M. Fleischhauer, A. Imamoglu, and J. P. Marangos, Electromagnetically induced transparency: Optics in coherent media, *Rev. Mod. Phys.* **77**, 633 (2005).
- [15] S. Chen, M. J. Bell, A. R. Beck, H. Mashiko, M. Wu, A. N. Pfeiffer, M. B. Gaarde, D. M. Neumark, S. R. Leone, and K. J. Schafer, Light-induced states in attosecond transient absorption spectra of laser-dressed helium, *Phys. Rev. A* **86**, 063408 (2012).
- [16] J. E. Bækhoj and L. B. Madsen, Light-induced structures in attosecond transient-absorption spectroscopy of molecules, *Phys. Rev. A* **92**, 023407 (2015).
- [17] C. Ott, A. Kaldun, P. Raith, K. Meyer, M. Laux, J. Evers, C. H. Keitel, C. H. Greene, and T. Pfeifer, Lorentz meets Fano in spectral line shapes: A universal phase and its laser control, *Science* **340**, 716 (2013).
- [18] A. Kaldun, C. Ott, A. Blättermann, M. Laux, K. Meyer, T. Ding, A. Fischer, and T. Pfeifer, Extracting Phase and Amplitude Modifications of Laser-Coupled Fano Resonances, *Phys. Rev. Lett.* **112**, 103001 (2014).
- [19] M. D. Crisp, Propagation of small-area pulses of coherent light through a resonant medium, *Phys. Rev. A* **1**, 1604 (1970).
- [20] G. L. Lamb, Analytical descriptions of ultrashort optical pulse propagation in a resonant medium, *Rev. Mod. Phys.* **43**, 99 (1971).
- [21] M. A. Bouchene, Phase control of dispersion effects for an ultrashort pulse train propagating in a resonant medium, *Phys. Rev. A* **66**, 065801 (2002).
- [22] D. Strasser, T. Pfeifer, B. J. Hom, A. M. Müller, J. Plenge, and S. R. Leone, Coherent interaction of femtosecond extreme-UV light with He atoms, *Phys. Rev. A* **73**, 021805(R) (2006).
- [23] J. C. Delagnes and M. A. Bouchene, Gain-dispersion coupling induced by transient light shifts in an atomic medium, *Phys. Rev. A* **76**, 023422 (2007).
- [24] A. N. Pfeiffer, M. J. Bell, A. R. Beck, H. Mashiko, D. M. Neumark, and S. R. Leone, Alternating absorption features during attosecond-pulse propagation in a laser-controlled gaseous medium, *Phys. Rev. A* **88**, 051402(R) (2013).
- [25] C.-T. Liao, A. Sandhu, S. Camp, K. J. Schafer, and M. B. Gaarde, Beyond the Single-Atom Response in Absorption Line Shapes: Probing a Dense, Laser-Dressed Helium Gas with Attosecond Pulse Trains, *Phys. Rev. Lett.* **114**, 143002 (2015).
- [26] C.-T. Liao, A. Sandhu, S. Camp, K. J. Schafer, and M. B. Gaarde, Attosecond transient absorption in dense gases: Exploring the interplay between resonant pulse propagation and laser-induced line-shape control, *Phys. Rev. A* **93**, 033405 (2016).
- [27] C.-T. Liao and A. Sandhu, XUV transient absorption spectroscopy: Probing laser-perturbed dipole polarization in single atom, macroscopic, and molecular regimes, *Photonics* **4**, 17 (2017).
- [28] Y. He, Z. Liu, Z. Cui, Y. Zhang, A. N. Pfeiffer, T. Pfeifer, J. Ding, and B. Hu, Signatures of self-modulation effects during pulse propagation in single-pulse absorption spectra, *Phys. Rev. A* **99**, 053418 (2019).
- [29] Y. He, R. Chen, F. Wang, A. N. Pfeiffer, Y. Zhang, Z. Cui, J. Ding, Z. Liu, and B. Hu, Macroscopic transient absorption in a V-type three-level system, *J. Phys. B: At., Mol. Opt. Phys.* **53**, 175601 (2020).
- [30] Y. He, Z. Liu, N. Xue, C. Ott, T. Pfeifer, A. N. Pfeiffer, and B. Hu, Watching the formation and reshaping of a Fano resonance in a macroscopic medium, *Phys. Rev. A* **103**, L041102 (2021).
- [31] R. Santra, V. S. Yakovlev, T. Pfeifer, and Z.-H. Loh, Theory of attosecond transient absorption spectroscopy of strong-field-generated ions, *Phys. Rev. A* **83**, 033405 (2011).
- [32] M. Chini, X. Wang, Y. Cheng, and Z. Chang, Resonance effects and quantum beats in attosecond transient absorption of helium, *J. Phys. B: At., Mol. Opt. Phys.* **47**, 124009 (2014).
- [33] S. H. Autler and C. H. Townes, Stark effect in rapidly varying fields, *Phys. Rev.* **100**, 703 (1955).
- [34] A. N. Pfeiffer and S. R. Leone, Transmission of an isolated attosecond pulse in a strong-field dressed atom, *Phys. Rev. A* **85**, 053422 (2012).
- [35] S. Yoshida, C. O. Reinhold, J. Burgdörfer, S. Ye, and F. B. Dunning, Photoexcitation of  $n \simeq 305$  Rydberg states in the presence of an rf drive field, *Phys. Rev. A* **86**, 043415 (2012).
- [36] M. B. Gaarde, C. Buth, J. L. Tate, and K. J. Schafer, Transient absorption and reshaping of ultrafast XUV light by laser-dressed helium, *Phys. Rev. A* **83**, 013419 (2011).
- [37] M. Lucchini, J. Herrmann, A. Ludwig, R. Locher, M. Sabbar, L. Gallmann, and U. Keller, Role of electron wavepacket interference in the optical response of helium atoms, *New J. Phys.* **15**, 103010 (2013).
- [38] X. Wang, M. Chini, Y. Cheng, Y. Wu, X.-M. Tong, and Z. Chang, Subcycle laser control and quantum interferences in attosecond photoabsorption of neon, *Phys. Rev. A* **87**, 063413 (2013).
- [39] S. Chen, M. Wu, M. B. Gaarde, and K. J. Schafer, Quantum interference in attosecond transient absorption of laser-dressed helium atoms, *Phys. Rev. A* **87**, 033408 (2013).

- [40] E. R. Warrick, J. E. Bækhoj, W. Cao, A. P. Fidler, F. Jensen, L. B. Madsen, S. R. Leone, and D. M. Neumark, Attosecond transient absorption spectroscopy of molecular nitrogen: Vibrational coherences in the  $b' \ ^1 \Sigma_u^+$  state, *Chem. Phys. Lett.* **683**, 408 (2017).
- [41] B. Bernhardt, A. R. Beck, X. Li, E. R. Warrick, M. J. Bell, D. J. Haxton, C. W. McCurdy, D. M. Neumark, and S. R. Leone, High-spectral-resolution attosecond absorption spectroscopy of autoionization in xenon, *Phys. Rev. A* **89**, 023408 (2014).
- [42] H. Xu, W. Cao, J. Zhang, Y. Mo, K. Mi, Z. Yang, Q. Zhang, and P. Lu, Mapping time-dependent quasi-energies of laser dressed helium, *Opt. Express* **29**, 11342 (2021).
- [43] A. Blättermann, C. Ott, A. Kaldun, T. Ding, and T. Pfeifer, Two-dimensional spectral interpretation of time-dependent absorption near laser-coupled resonances, *J. Phys. B: At., Mol. Opt. Phys.* **47**, 124008 (2014).
- [44] Z. Liu, Q. Wang, J. Ding, S. M. Cavaletto, T. Pfeifer, and B. Hu, Observation and quantification of the quantum dynamics of a strong-field excited multi-level system, *Sci. Rep.* **7**, 1 (2017).